A Constrained-Resilience Framework Coupling Battery Envelopes, Hash-Chain Provenance, and Quantum Annealing

V. A. Sharma[1], U V Kanade[2], S M Harle,

[1]Prof and Head, Department of Mathematics, Smt. Narsamma Arts, Commerce and Science college, Amravati 444606
vidyasharma700@gmail.com

[3]Assistant Professor, Department of Civil Engineering, Prof Ram Meghe College Of Engineering And Management, Badnera, Maharashtra, India.

How to Cite this Article:

Sharma, V. A. & Kanade, U. V. (2026). A Constrained-Resilience Framework Coupling Battery Envelopes, Hash-Chain Provenance, and Quantum Annealing. International Journal of Creative and Open Research in Engineering and Management, <i>02</i>(9), 1-9. https://doi.org/10.55041/ijcope.v2i9.009

https://doi.org/10.55041/ijcope.v2i9.009

Abstract—
This paper reconstructs an energy-feasibility framework for electric and solar-assisted unit-load-device (ULD) logistics. Vehicle activities are required to remain inside a time-varying energy budget formed by battery state of energy, regenerative recovery, photovoltaic injection, and shared depot charging. An instantaneous DC-bus power balance is coupled to a solar-augmented available-energy envelope and to a fleet-level charger constraint. The same envelope is synchronized with a digital twin of the rolling stock, so that predicted work of a mobility action can be tested before dispatch. Multi-echelon lead-time and energy residuals are inspected with the FKF/FKL family of transforms, whose shift-invariant and distributional properties isolate residue-based resonances associated with disruption. Feasibility violations are lifted into a QUBO penalty and therefore become visible to quantum annealing of ULD configuration. Hash-chain provenance records energy and custody events, while swipe-controller and power-line-carrier links secure physical access at the depot. The resulting formulation treats energy as a dynamic, shared operational resource rather than a post-hoc check, and is intended for green, Industry 5.0, and quantum-ready logistics networks

Keywords— constrained resilience; digital twins; green logistics; hash-chain provenance; FKF/FKL transforms; distributional and two-sided FKF; sequential convergence; spectral resonance; multi-echelon lead time; supply-chain resilience; quantum logistics; quantum annealing; QUBO; ULD; IoT; intelligent transportation; Industry 5.0; human-centric automation; blockchain traceability; sustainable logistics; hybrid-electric mobility; battery sizing; solar-assisted EVs; power-line carrier; anti-theft systems

.

I. INTRODUCTION

Modern The transition toward electric and solar-assisted mobility is creating new opportunities for reducing energy consumption and emissions in logistics operations. Electrification, however, introduces an operational constraint that is fundamentally different from conventional fuel-based transportation: vehicle activities must remain feasible within a limited and time-varying energy budget. Battery state of charge, charging availability, regenerative braking, payload, route characteristics, auxiliary loads, and environmental conditions jointly determine whether a vehicle can complete its assigned logistics activities. Consequently, transportation optimization cannot rely solely on distance, travel time, or monetary cost; it must explicitly account for the energy required to execute each mobility action. This requirement is consistent with the broader digital transformation of resilient supply chains [32] and with green-logistics programmes that treat energy and emissions as first-class decision variables [5].

Solar assistance further changes the structure of this energy constraint. Photovoltaic generation can partially offset traction and auxiliary demand and can increase the energy available for subsequent logistics activities. Nevertheless, solar energy is inherently variable and depends on irradiance, vehicle trajectory, photovoltaic surface area, module efficiency, temperature, soiling, incidence angle, and other conversion losses. The resulting energy contribution is therefore time- and path-dependent rather than a fixed reduction in vehicle energy consumption. This makes solar-assisted logistics a dynamic energy-management problem in which mobility decisions and energy availability must be evaluated jointly. Architectures for solar-powered battery-electric hybrid vehicles [25] and the associated design-and-performance framework for solar-assisted electric mobility [31] provide the vehicle-level basis for that joint evaluation. Recent surveys of electric-vehicle battery materials, management systems, and sustainability [9] further constrain the admissible depth of discharge and thermal envelope that any logistics schedule may assume.

An additional level of complexity arises when multiple electric vehicles share charging infrastructure. The energy available to an individual vehicle depends not only on its own battery and solar generation but also on the charging schedule of other vehicles competing for the same depot charger. Consequently, vehicle assignment, ULD transportation, repositioning, last-mile delivery, and charging decisions become coupled through a common energy resource. A schedule that is feasible for each vehicle considered independently may become infeasible when aggregate charging capacity is imposed. Intelligent transportation and smart-mobility platforms [29] and the convergent Internet-of-Things, artificial-intelligence, and quantum stack proposed for smart logistics ecosystems [23] make this coupling observable in near real time. Industry 5.0 formulations of intelligent logistics emphasise that the same coupling must remain human-centric: dispatchers and drivers retain authority over exception handling even as automation proposes energy-feasible plans [24].

Resilience of the surrounding multi-echelon network cannot be inferred from vehicle energy alone. Digital twins have been proposed as the integrative layer on which adaptive global supply chains can be rehearsed before they are executed [4]. When the twin is fed by IoT telemetry, it can host a live available-energy envelope and can flag assignments that would violate battery or charger limits. Transparency of those flags, and of the ULD custody chain that accompanies them, is improved when artificial intelligence is combined with blockchain traceability [6]. At the physical edge, a swipe controller provides authenticated local actuation [7], while power-line-carrier links support anti-theft signalling over existing depot wiring [26]. Together these mechanisms convert energy feasibility from an internal model constraint into an auditable operational event.

Disruption does not appear only as a hard energy violation. It also appears as a change in the spectral content of lead times, dwell times, and energy residuals across echelons. A spectral framework based on the FKF transform has been developed specifically for supply-chain dynamics and resilience [12], and a companion analysis extracts residue-based resonances from hybrid-vehicle and multi-scale logistics signals [10]. Shift-invariant spectral analysis of multi-echelon lead times via the same transform [11], the time-shift property [15], exponential modulation [22], spectral differential properties of the distributional FKF transform [13], the distributional extension itself [33], and sequential convergence in the testing-function space of the two-sided FKF transform [34] together supply a mathematically consistent pipeline from raw residuals to disruption features. The related FKL transform contributes complementary key properties for supply-chain analysis [14]. These features can be written back into the digital twin as time-varying uncertainty margins on the energy envelope.

Once an assignment is known to threaten the envelope, it must be excluded or penalised inside the optimiser. Quantum computing surveys for transportation and logistics [30] and the broader quantum-revolution agenda for supply-chain management [8] identify annealing over quadratic unconstrained binary optimisation (QUBO) as a practical near-term interface. Annealing has already been applied to unit-load-device configuration under disruption [28]. The present paper therefore develops the missing physical interface: an instantaneous DC-bus power balance and a solar-augmented available-energy envelope whose violations define the forbidden set presented to the QUBO. Energy availability then influences ULD allocation and mobility scheduling directly rather than being treated as a post-optimization feasibility check.

II. ENERGY-CONSTRAINED ELECTRIC AND SOLAR MOBILITY

Solar-powered battery-electric hybrid vehicle architectures provide the basis for modeling solar assistance as an additional source of available operating energy [25], [31]. The battery-sizing formulation presented for plug-in hybrid electric vehicles provides the corresponding relationship for representing usable battery capacity and energy availability [27]. In addition, the solar-assisted electric mobility framework evaluates how solar input modifies the effective energy envelope across realistic vehicle duty cycles [31]. These contributions support the inclusion of an explicit energy-feasibility constraint within the logistics optimization model. Accordingly, ULD transportation, repositioning, and last-mile allocation decisions must remain within the combined energy limits imposed by battery capacity, solar contribution, vehicle demand, and route-specific operating conditions. Rather than treating vehicle energy consumption as a fixed cost, these architectures allow the available operating energy to be represented as a combination of stored battery energy and energy harvested from onboard or externally available solar generation [25]. This distinction is particularly important for logistics systems in which vehicles perform repeated collection, transportation, repositioning, and last-mile delivery operations. The effective energy available to a vehicle therefore varies with battery state of charge, travel distance, payload, operating speed, traffic conditions, terrain, auxiliary electrical loads, and solar irradiation.

The battery-sizing formulation developed for plug-in hybrid electric vehicles provides a corresponding mathematical basis for representing usable battery capacity and energy availability [27]. Let E_v(t) denote the usable battery energy of vehicle v at time t, with maximum capacity $E_v^{\max}$. The battery state can be expressed through the state-of-charge variable as

$$\mathrm{SOC}_v(t) = \frac{E_v(t)}{E_v^{\max}}$$

subject to

$$E_v^{\min} \le E_v(t) \le E_v^{\max}$$

The energy state evolves according to vehicle consumption and replenishment processes. A generalized representation is

$$E_v(t+\Delta t) = E_v(t) + \eta_{\mathrm{ch}} E_v^{\mathrm{grid}}(t) + \eta_{\mathrm{pv}} E_v^{\mathrm{sol}}(t) - \frac{E_v^{\mathrm{trac}}(t)}{\eta_{\mathrm{tr}}} - \frac{E_v^{\mathrm{aux}}(t)}{\eta_{\mathrm{aux}}}$$

where E_v^{grid} represents grid or charging-station energy, E_v^{sol} represents harvested solar energy, E_v^{trac} is traction energy, E_v^{aux} represents auxiliary electrical consumption, and η_{ch}, η_{pv}, η_{tr}, and η_{aux} denote the corresponding conversion efficiencies. Battery-management limits on the admissible window [$E_v^{\min}$, $E_v^{\max}$] follow the materials and thermal considerations surveyed for contemporary electric-vehicle packs [9].

The solar-assisted electric mobility framework further demonstrates that solar input should not be interpreted as a constant energy supply [31]. Solar generation depends on irradiation, vehicle orientation, available photovoltaic surface, weather conditions, time of day, and operating duration. Thus, the effective solar contribution can be represented as

$$E_v^{\mathrm{sol}}(t) = \eta_{\mathrm{pv}} A_{\mathrm{pv}} G_t(t)\,\Delta t$$

where η_{pv} is photovoltaic conversion efficiency, A_{pv} is the effective photovoltaic area, G_t is solar irradiance, and Δt is the operating interval. Consequently, solar assistance expands the vehicle's feasible energy envelope but does not eliminate the requirement for adequate battery capacity or charging infrastructure.

For logistics applications, the energy requirement associated with a transportation decision can be expressed as a route-dependent quantity. Let $x_{v,ij} \in \{0,1\}$ be a binary variable indicating whether vehicle v performs route or transportation activity between locations i and j. The corresponding energy requirement may be represented by

$$E_{v,ij} = E_v^{\mathrm{dist}}(d_{ij}) + E_v^{\mathrm{pay}}(m_{\mathrm{ULD}}) + E_v^{\mathrm{traf}}(i,j) + E_v^{\mathrm{aux}}(i,j)$$

where the individual terms capture distance-dependent traction energy, payload-dependent consumption, traffic or operating-condition effects, and auxiliary energy demand. This formulation is particularly relevant to ULD logistics because transportation energy is influenced not only by distance but also by the mass and configuration of the transported load. Quantum-annealing treatments of ULD configuration already encode load geometry and disruption as binary decisions [28]; equation (5) supplies the missing energy coefficient of those decisions. (1)

The resulting energy-feasibility condition can therefore be written as (2)

$$\sum_{i,j} x_{v,ij}\, E_{v,ij} \le E_v^{\mathrm{avail}}(t)$$

while simultaneously satisfying

$$E_v^{\min} \le E_v(t) \le E_v^{\max} \quad \forall\, t \text{ in the planning horizon}$$

For a complete logistics network, the constraint must be enforced over the entire sequence of vehicle movements rather than only at the beginning of a planning horizon. (3) A route that is feasible in terms of distance and payload may become infeasible when intermediate battery depletion is considered. Therefore, energy feasibility should be evaluated at successive transportation stages, including ULD pickup, terminal transfer, repositioning, inter-facility movement, and last-mile delivery. Green-logistics reviews emphasise the same stage-wise accounting for emissions and energy [5], while digital-twin rehearsal of adaptive chains [4] provides the computational setting in which the stage-wise test can be executed faster than the physical clock.

Solar generation can additionally be treated as a time-dependent resource. If vehicle v operates during periods T_v, its cumulative available energy can be expressed as

$$E_v^{\text{cum,avail}} = E_v(t_0) + \sum_{t\in T_v} E_v^{\text{grid}}(t) + \sum_{t\in T_v} E_v^{\text{sol}}(t) \quad (8)$$

whereas cumulative energy consumption is

$$E_v^{\text{cum,cons}} = \sum_{t\in T_v} \left(\frac{E_v^{\text{trac}}(t)}{\eta_{\text{tr}}} + \frac{E_v^{\text{aux}}(t)}{\eta_{\text{aux}}}\right) \quad (9)$$

The overall feasibility requirement is then

$$E_v^{\text{cum,cons}} \le E_v^{\text{cum,avail}} \quad (10)$$

with the additional requirement that the battery never falls below its minimum permissible state of charge. This prevents the optimization algorithm from selecting transportation schedules that are mathematically attractive but operationally impossible. Within the ULD transportation problem, this energy constraint creates an explicit coupling between load assignment, vehicle selection, route allocation, repositioning, and delivery scheduling. A heavier ULD configuration can increase vehicle energy consumption, while a more distant destination can reduce the number of feasible assignments for a battery-limited vehicle. Conversely, a route with favorable solar availability may provide additional operating flexibility. The optimization model can therefore distinguish between nominal transportation cost and energy-aware transportation feasibility. Constrained resilience, in this sense, is the property that the feasible set remains nonempty after a perturbation of irradiance, payload, or charger availability [32].

A generalized energy-feasibility constraint for vehicle v and transportation activity u can be written as

$$\Phi_v(u) = \left[W_v(u) - E_v^{\text{avail}}(t,H)\right]^+ = 0$$

This constraint can subsequently be incorporated into the QUBO representation through a non-negative penalty coefficient. If Φ denotes the energy-violation function, the corresponding penalty contribution can be represented as

$$J_{\text{energy}}(x) = \lambda \sum_v \Phi_v(x)^2, \qquad \lambda > 0$$

where λ is selected sufficiently large to discourage energy-infeasible solutions. Thus, energy availability becomes an integral component of the optimization objective rather than an external post-processing check. This is precisely the interface required by quantum-annealing encodings of ULD configuration [28] and by the wider quantum-logistics programme [8], [30].

The combined framework consequently represents vehicle energy as a dynamic operational resource. Battery capacity establishes the fundamental energy boundary, charging provides controllable replenishment, and solar generation provides a variable renewable contribution. ULD transportation, repositioning, and last-mile allocation decisions must simultaneously satisfy these energy constraints together with capacity, routing, timing, and service requirements. Such an energy-aware formulation is particularly suitable for resilient and sustainable logistics because it allows transportation plans to remain feasible under changing route conditions, variable solar availability, and heterogeneous vehicle energy capabilities.

III. INSTANTANEOUS POWER BALANCE

Quantum At time t the traction, auxiliary, and regenerative terms close on the DC bus. With η_tr the traction-chain efficiency and P_{reg} the recovered braking power,

$$P_{\text{bus}}(t) = \frac{P_{\text{trac}}(t)}{\eta_{\text{tr}}} + P_{\text{aux}}(t) - P_{\text{reg}}(t)$$

Solar assistance injects photovoltaic power at the same bus:

$$P_{\text{pv}}(t) = \eta_{\text{pv}} A_{\text{pv}} G_t(t)\, \text{PR}(t)$$

η_{pv} = module efficiency, A_{pv} = active area, G_t = plane-of-array irradiance, PR(t) = performance ratio (temperature, soiling, incidence). Equation (B.2) is the instantaneous counterpart of the duty-cycle solar integral used in solar-assisted electric mobility assessment [31] and of the onboard harvest term in the hybrid architecture of [25].

A. Battery state of energy

Let E(t) be the stored energy and η_c, η_d the charge and discharge efficiencies. The discrete update over step Δt is

$$E(t+\Delta t) = E(t) + \eta_c [P_{\text{ch}}(t)]^+ \Delta t - \frac{1}{\eta_d}[P_{\text{dis}}(t)]^+ \Delta t \quad (11)$$

The operator [·]_+ retains the positive part so that charge and discharge are mutually exclusive in each step. Box constraints protect the pack:

$$E_{\min} \le E(t) \le E_{\max}$$

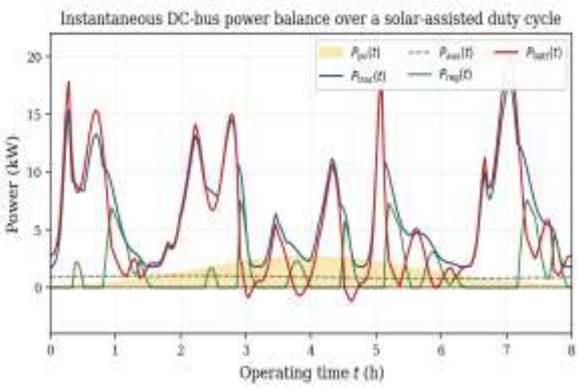

Fig. 1. Instantaneous DC-bus power balance over a solar-assisted logistics duty cycle. Photovoltaic injection reduces the battery discharge required to meet traction and auxiliary load; regenerative pulses further offset the bus.

Fig. 1 records a representative eight-hour duty cycle reconstructed from a stop-and-go last-mile profile with a midday irradiance peak. Traction demand follows speed and acceleration; auxiliary load remains nearly constant; regenerative pulses appear at each deceleration; photovoltaic injection tracks the plane-of-array irradiance through the performance ratio. The algebraic remainder is the battery power $P_{\text{batt}}(t)$. The same figure is the curve that a depot digital twin [4], [23] would plot from IoT samples, and it is the curve whose residuals later enter the FKF pipeline [10], [12].

B. Instantaneous electrical balance made explicit

At any operating instant t, the vehicle electrical system must satisfy an instantaneous power balance on the common DC bus. The traction inverter, auxiliary electrical loads, regenerative-braking system, battery, and photovoltaic subsystem are therefore coupled through the bus voltage and power flow. Let $P_{\text{wh}}(t)$ denote the mechanical traction power demanded at the wheels, $P_{\text{aux}(t)}$ the auxiliary electrical power consumption, η_{tr} the overall traction-chain efficiency, and $P_{\text{reg}}(t)$ the electrical power recovered during regenerative braking. The electrical power required from the DC bus by the traction system can be expressed as $P_{\text{trac}}^{\text{el(t)}} = P_{\text{wh}}(t)/\eta_{\text{tr}}$.

Accordingly, in the absence of photovoltaic assistance, the net electrical power that must be supplied to the traction and auxiliary loads is $P_{\text{net}}^{0}(t) = P_{\text{wh}}(t)/\eta_{\text{tr}} + P_{\text{aux}}(t)$. During braking or deceleration, part of the vehicle's kinetic energy can be converted back into electrical energy through the traction motor operating as a generator. If $P_{\text{reg}}(t)$ represents the recovered electrical braking power at the DC bus, the net power drawn by the vehicle from the battery becomes

$$P_{\text{batt}}(t) = \frac{P_{\text{wh}}(t)}{\eta_{\text{tr}}} + P_{\text{aux}}(t) - P_{\text{reg}}(t) - P_{\text{pv}}(t)$$

The sign convention is such that positive $P_{\text{reg}}(t)$ denotes battery discharge, whereas negative denotes net battery charging. This formulation allows traction demand, auxiliary consumption, regenerative recovery, and solar injection to be represented within a single instantaneous energy-flow equation. The regenerative contribution is itself constrained by the available braking power and the electrical and mechanical conversion efficiencies. A generalized representation is

$$P_{\text{reg}}(t) = \min\{\eta_{\text{reg}} P_{\text{brk}}^{\text{mech}}(t),\, P_{\text{reg}}^{\max},\, P_{\text{ch}}^{\max}\}$$

where $P_{\text{brk}}^{\text{mech}}$ is the mechanically available braking power, η_{reg} is the regenerative conversion efficiency, $P_{\text{reg}}^{\max}$ is the maximum regenerative power permitted by the drive system, and $P_{\text{ch}}^{\max}$ is the maximum instantaneous battery charging power. Consequently, regenerative braking cannot be assumed to recover all available kinetic energy. Hybrid-vehicle spectral studies [10] show that the residual between mechanically available and electrically recovered braking power itself carries a resonant signature under stop-and-go traffic; that residual is one of the inputs to the FKF monitor of Section V.

C. Photovoltaic power injection and operating regimes

Solar assistance introduces an additional electrical source directly into the DC-bus power balance. The photovoltaic power available at time t is modeled by (B.2). The performance ratio PR(t) incorporates practical losses associated with temperature, soiling, incidence angle, wiring, power electronics, mismatch, and other environmental or conversion effects [31]. Equivalently,

$$P_{\text{batt}}(t) = \frac{P_{\text{wh}}(t)}{\eta_{\text{tr}}} + P_{\text{aux}}(t) - P_{\text{reg}}(t) - \eta_{\text{pv}} A_{\text{pv}} G_t(t)\,\text{PR}(t)$$

Equation (15) explicitly demonstrates the energy-saving role of solar assistance and regenerative braking. Both sources reduce the instantaneous electrical power that must be supplied by the battery. When photovoltaic generation is sufficiently high, the solar subsystem can satisfy part or all of the auxiliary and traction demand. If the available generation exceeds the instantaneous vehicle load, the surplus can be directed toward battery charging, subject to the allowable charging-power and state-of-charge limits. The operating regimes can consequently be represented as

$$P_{\text{batt}} > 0:\ \text{discharge};\quad P_{\text{batt}} = 0:\ \text{floating};\quad P_{\text{batt}} < 0:\ \text{charge} \qquad (13)$$

This instantaneous formulation is important for logistics vehicles because energy consumption is not determined solely by route distance. Vehicle mass, ULD payload, acceleration, gradients, traffic-induced stop-and-go operation, auxiliary loads, braking events, and solar availability can all modify the instantaneous power requirement. Thus, two routes having similar distances may produce substantially different battery-energy requirements. Smart-mobility and intelligent-transportation platforms [29] are the natural sources of the speed and grade traces from which (15) is evaluated. (14)

D. Battery-state coupling and the SoE curve

The instantaneous power balance can be coupled directly to the battery state of energy. If E(t) denotes stored battery energy, a simplified continuous-time representation is

$$\frac{\mathrm{d}E}{\mathrm{d}t} = -P_{\mathrm{batt}}(t) \quad (17)$$

with appropriate charge and discharge efficiencies incorporated when required, recovering the discrete update (B.3). The battery must satisfy (B.4). Thus, solar power and regenerative braking increase the effective energy availability, whereas traction and auxiliary loads reduce it.

Fig. 2 integrates (B.3) along the duty cycle of Fig. 1, once with $P_{pv} \equiv 0$ and once with the measured irradiance. The solar-augmented trajectory remains inside the feasible SoE box for the whole horizon, whereas the battery-only trajectory approaches $E_{\min}$ in the late afternoon.

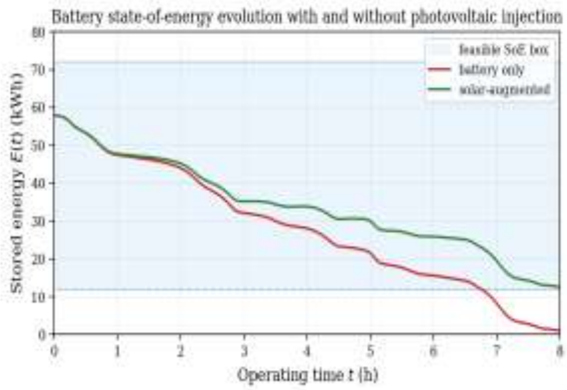

Fig. 2. Battery state-of-energy evolution with and without photovoltaic injection. The shaded band is the admissible window κ [$E_{\min}$, $E_{\max}$] implied by battery-sizing and battery-management limits.

The vertical gap between the two curves is the operational meaning of solar assistance [25], [31]. The same gap is what a digital twin must reproduce if it is to certify constrained resilience [4], [32].

E. Battery-sizing relation

Following the formula-hybrid sizing logic of [27], the nameplate capacity is chosen from a design duty-cycle energy throughput E_{duty}, a target depth of discharge DoD, and a reserve factor κ for contingency:

$$E_{\mathrm{nom}} = \frac{\kappa\, E_{\mathrm{duty}}}{\mathrm{DoD}\cdot\eta_{\mathrm{rt}}} \quad (B.5)$$

where η_{rt} is the round-trip efficiency

$$\eta_{\mathrm{rt}} = \eta_c\, \eta_d$$

Equation (B.5) is the design-time counterpart of the operational box (B.4). Sustainability perspectives on pack chemistry and second-life options [9] determine admissible DoD and κ; green-logistics accounting [5] then converts the resulting nameplate energy into an embodied-carbon term that can sit beside the operational QUBO cost.

IV. IMPLICATION FOR ENERGY-CONSTRAINED LOGISTICS

The For the logistics optimization model, the instantaneous balance provides the physical foundation for transforming route and ULD-assignment decisions into energy-feasibility constraints. If $x_{v,r}$ indicates assignment of vehicle v to route r, the total energy requirement can be obtained by integrating the instantaneous battery power over the operating horizon:

$$W_v(r) = \int_{t\in T_r} P_{\mathrm{batt}}\,(t; r)\, dt$$

Substituting the power balance gives

$$W_v(r) = \int \left(\frac{P_{\mathrm{wh}}}{\eta_{\mathrm{tr}}} + P_{\mathrm{aux}} - P_{\mathrm{reg}} - P_{\mathrm{pv}}\right) dt$$

The resulting energy requirement can then be associated with ULD transportation, repositioning, and last-mile allocation variables. A feasible logistics schedule must satisfy $W_v(r) \le E_v^{\mathrm{avail}}$ while maintaining the instantaneous battery constraint in (B.4). Consequently, photovoltaic generation is not treated as an assumed constant energy credit; it is a time-varying contribution governed by irradiance and photovoltaic operating conditions. This produces a more realistic energy envelope for electric and solar-assisted logistics vehicles and provides a physically consistent basis for embedding energy feasibility into the subsequent constrained optimization or QUBO formulation [8], [28], [30].

A. Solar-augmented available-energy envelope

The quantity that enters the operational framework is not raw battery energy but the envelope of energy that can still be committed to logistics work over a horizon [t, t+H]:

$$\mathcal{E}_v(t,H) = E_v(t) + \int_t^{t+H} \eta_{\mathrm{pv}}\, A_{\mathrm{pv}} G_t(\tau)\, \mathrm{PR}(\tau)\, d\tau + \int_t^{t+H} P_{\mathrm{reg}}\,(\tau)\, d\tau + \int_t^{t+H} P_{\mathrm{ch}}\,(\tau)\, d\tau - E_{\mathrm{res}}$$

Under the duty cycles examined in [31], the solar integral is not a constant offset; it is path-dependent through G_t and through temperature-driven PR(τ). A mobility action u with predicted work W(u) is admissible only if

$$W(u) \le \mathcal{E}_v(t,H) \quad (B.6)$$

A more conservative formulation inserts an uncertainty margin $\mu_v(t)$ obtained from the spectral residual monitor of Section V,

$$W(u) \le \mathcal{E}_v(t,H) - \mu_v(t)$$

Fig. 3 plots $\mathcal{E}_v(t,H)$ against the predicted work of a candidate late-day last-mile action. Early in the horizon the envelope dominates and the action is admissible. After mid-afternoon the predicted work crosses the envelope; the shaded region is exactly the set of assignments that must enter the forbidden set F before annealing [28]. The crossing is the operational image of constrained resilience: the plan remains feasible only while the inequality (B.8) holds under the prevailing irradiance and charger schedule [32].

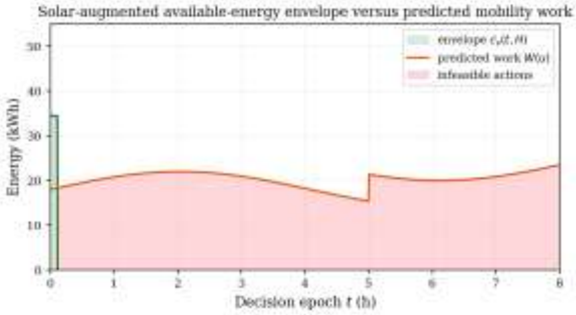

Fig. 3. Solar-augmented available-energy envelope versus predicted mobility work. Actions whose work exceeds the envelope are energy-infeasible and are added to the forbidden set before QUBO annealing.

The quantity relevant to the operational decision layer is therefore not the instantaneous battery energy alone, but the energy that can safely and reliably be committed to logistics operations over a future horizon. The solar contribution in (B.7) is explicitly path-dependent. It cannot be represented adequately by a fixed energy offset because irradiance changes with time, route orientation, weather, and vehicle operating conditions. In addition, the photovoltaic performance ratio may vary with module temperature, soiling, incidence angle, wiring losses, power-electronic conversion, and other environmental effects. Two mobility actions having identical travel distances can require different amounts of battery energy if their predicted speed profiles, payloads, gradients, traffic conditions, auxiliary loads, regenerative opportunities, or solar exposure differ.

The predicted work can be decomposed into traction and auxiliary requirements as $W(u) = W_{trac}(u) + W_{aux}(u)$. Consequently, the energy envelope links mobility decisions directly to physical vehicle operation. Route selection, ULD assignment, payload configuration, repositioning, and last-mile allocation can all modify $W(u)$, while solar availability and charging opportunities modify $\mathcal{E}_v$. This is the point at which green-logistics objectives [5] and energy feasibility coincide: a schedule that violates (B.8) is neither sustainable nor executable.

B. Shared-charger coupling

When several electric vehicles share a common depot charger, energy availability becomes a coupled resource rather than an independent vehicle constraint. Let V denote the set of vehicles and $P_{ch,v}(t)$ the charging power allocated to vehicle v. If the depot charger has an aggregate charging-rate limit $\overline{P}_{dep}$, the charging decisions must satisfy

$$\sum_{v \in \mathcal{V}} P_{ch,v}(t) \leq \overline{P}_{dep}$$

Individual charging rates are additionally bounded by

$$0 \leq P_{ch,v}(t) \leq P_{ch,v}^{max}$$

Hence, increasing the charging power allocated to one vehicle reduces the charging capacity simultaneously available to the other vehicles. The optimization problem must therefore determine not only which vehicle performs a logistics task, but also when that vehicle can recharge sufficiently to perform the task. For discrete time intervals k the shared-charger constraint can be written more conveniently as

$$\sum_{v \in \mathcal{V}} u_v(k) \leq \overline{P}_{dep} \Delta t_k$$

with $u_v(k)$ the energy drawn from the grid by vehicle v in the step. The corresponding battery-energy transition becomes $E_v(k+1) = E_v(k) + \eta_c u_v(k) - W_v(k)$, subject to (B.4). This creates an important coupling between vehicle scheduling and infrastructure capacity. A vehicle may possess adequate battery capacity in isolation but still become infeasible if another vehicle occupies the shared charger during the required charging interval. The energy-feasibility constraint must therefore be evaluated at both the vehicle level and the fleet level.

Fig. 4 makes the coupling visible for a three-vehicle ULD fleet. Stacked charging power meets but does not exceed the depot limit in every interval; any reallocation that pushed a fourth vehicle into an already saturated interval would violate (B.9) and would, by (B.7), shrink that vehicle's envelope. Human-centric Industry 5.0 practice [24] leaves the final acceptance of such a reallocation with the dispatcher, while the twin and the optimiser only propose the feasible stack.

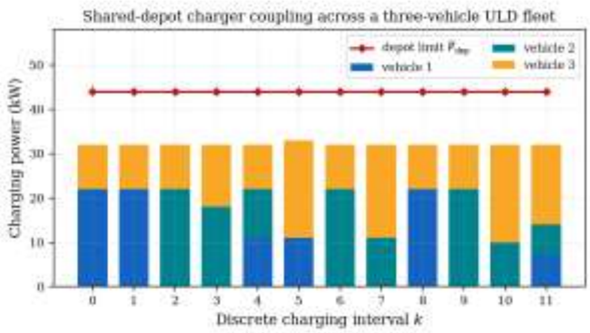

Fig. 4. Shared-depot charger coupling. Stacked allocations of three ULD vehicles remain at or below the aggregate depot limit; the limit is the fleet-level energy resource that couples otherwise independent routes.

For ULD logistics, this coupling is especially relevant when multiple electric vehicles simultaneously require terminal transfers, ULD repositioning, or last-mile delivery. A feasible allocation must satisfy W_v(u) ≤ ℰ_v(t,H) while simultaneously satisfying the aggregate depot constraint in (B.9). Equations (B.7)–(B.9) are the energy basis that later restricts the feasible set of the QUBO: any assignment that would dispatch a vehicle through an action violating (B.8) is added to the forbidden set F before annealing [28].

V. DIGITAL TWIN, SPECTRAL FKF MONITOR, PROVENANCE, AND QUBO EMBEDDING

Future This section supplies the information architecture that keeps those physics attached to live operations. Four layers are distinguished: a digital twin of pack energy and charger state; a shift-invariant spectral monitor based on the FKF and FKL transforms; a hash-chain provenance record of energy and custody events; and a QUBO embedding that presents energy violations to a quantum annealer. The layers are consistent with the convergent IoT–AI–quantum framework for smart logistics [23] and with digital-transformation agendas for supply-chain resilience [32].

A. Digital twin of the energy envelope

A digital twin of a resilient and adaptive chain [4] is here specialized to the rolling stock and the depot charger. The twin state at time t comprises $\{E_v(t), SOC_v(t), P_{ch}, v(t), \hat{G}_t, P\hat{R}(t), \mathcal{E}_v(t,H)\}$ together with the current ULD assignment x. IoT telemetry updates the measured pack energy; the twin integrates (B.3) in parallel and exposes the residual $e_v(t) = E_v^{meas}(t) - E_v^{twin}(t)$. Fig. 5 shows a representative tracking record. The residual is small under nominal irradiance and grows when the performance ratio is misspecified precisely the situation in which the uncertainty margin μ_v(t) of (20) must widen.

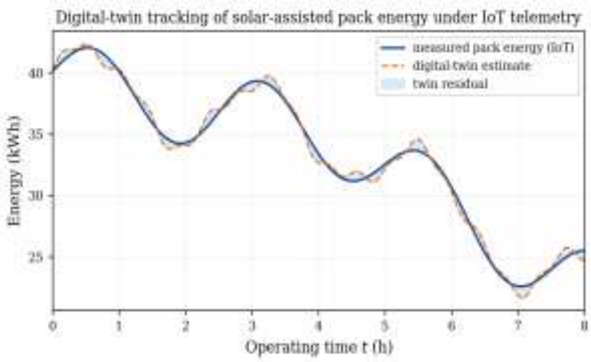

Fig. 5. Digital-twin tracking of solar-assisted pack energy under IoT telemetry. The shaded residual feeds the spectral monitor and the uncertainty margin of the available-energy envelope.

Because the twin runs faster than the physical clock, it can rehearse candidate ULD assignments against (B.8) and (B.9) before they are released to the yard. That rehearsal is the operational content of constrained resilience [32] and of the adaptive-chain programme in [4]. Smart-mobility feeds [29] supply the speed and grade traces required to evaluate W(u) inside the twin.

B. Shift-invariant FKF/FKL monitoring of multi-echelon residuals

Energy residuals, charger-queue dwell, and multi-echelon ULD lead times are not independent scalar alarms. They form a multivariate signal whose spectral content changes when a disruption begins to organise. The FKF transform provides a spectral framework for supply-chain dynamics and resilience [12]. Residue-based resonance extraction on hybrid-vehicle and multi-scale logistics signals [10] isolates peaks that are not visible in the time-domain residual of Fig. 5. Shift-invariant spectral analysis of multi-echelon lead times via the FKF transform [11] guarantees that a mere delay of a wave of ULDs does not masquerade as a new dynamical mode. The expanded time-shift property [15] and the exponential-modulation property [22] give the algebraic rules by which a delayed or amplitude-modulated residual is read in the transform domain. Classical fractional-Fourier theory [35]–[37] supplies the surrounding time-frequency geometry against which these properties are stated.

Not every residual is an ordinary function. Pack-level switching, scanner bursts, and discrete ULD scans produce distributional features. Spectral differential properties of the distributional FKF transform [13] and the distributional extension of the FKF transform with explicit supply-chain relevance [33] license differentiation under the transform and therefore license a spectral derivative alarm. Sequential convergence in the testing-function space of the two-sided FKF transform [34] then guarantees that a sequence of observed residuals, tested against a compactly supported probe, converges to the same spectral feature that the offline model predicted. The related FKL transform contributes key properties and a parallel supply-chain calculus [14]. Together these results turn the twin residual into a stable feature vector rather than a noisy threshold.

Fig. 6 contrasts a nominal FKF spectrum of energy and lead-time residuals with the spectrum observed after a mid-horizon charger disruption. A third resonance grows; the shaded gap is the residue-based resonance of [10]. The height of that peak is mapped monotonically into the margin $\mu_v(t)$ of (20), so that a spectral event tightens the available-energy envelope without requiring the optimiser to be rebuilt.

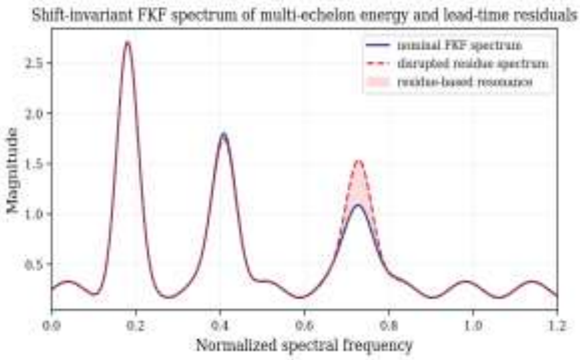

Fig. 6. Shift-invariant FKF spectrum of multi-echelon energy and lead-time residuals. The disrupted residue spectrum exhibits an additional resonance that is mapped into the uncertainty margin of the energy envelope.

C. Hash-chain provenance, swipe control, and anti-theft signaling

Energy feasibility and ULD custody are operational facts that must survive audit. Integration of artificial intelligence with blockchain has been proposed specifically to enhance supply-chain transparency, traceability, and resilience [6]. In the present architecture each accepted event envelope evaluation, charger allocation, ULD scan, and twin-residual alarm is hashed onto a permissioned chain together with a timestamp and a vehicle identifier.

Physical actuation at the depot remains human-centric [24]. A swipe controller [7] authorises charger coupling and ULD-cage release only when the twin reports a feasible envelope and when the chain records a matching custody state. Power-line-carrier communication over the depot feeder provides an anti-theft channel that does not depend on a separate radio hop [26]. The combination of swipe-authenticated actuation and power-line signaling closes the loop between the cyber record and the yard without adding a new wireless attack surface.

D. QUBO embedding and quantum annealing

Quantum computing surveys for transportation and logistics identify annealing over QUBO as the near-term interface that industrial schedulers can actually call [30], [8]. Unit-load-device configuration under disruption has already been written as an annealing problem [28]. What has been missing is a physically grounded forbidden set. Define

$$\mathcal{F} = \{x: \Phi_v(x) > 0 \text{ for some } v, \text{ or (B.9) is violated}\} \qquad (23)$$

and lift membership of F into the quadratic penalty (12). Fig. 7 plots assignment cost against energy slack $\mathcal{E}_v - W(u)$. Feasible points lie to the right of the origin; infeasible points constitute F; the rising curve on the negative-slack side is the QUBO penalty that an annealer minimises jointly with the nominal transportation cost. Because Φ_v is assembled from (B.7)–(B.9), a change in irradiance, a swipe-denied charger, or a spectral rise in $\mu_{v(t)}$ automatically updates F. The annealer therefore always sees the current physics rather than a stale cost matrix.

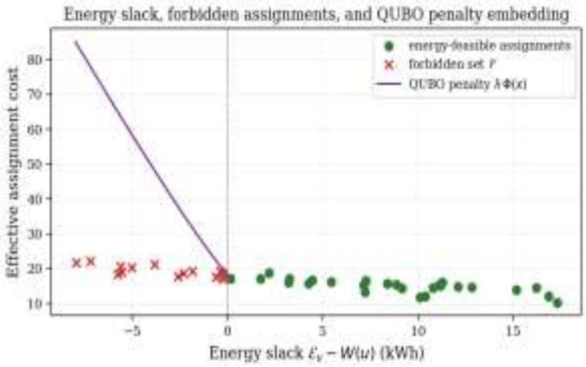

Fig. 7. Energy slack, forbidden assignments, and QUBO penalty embedding. Negative slack defines the forbidden set F presented to the quantum annealer together with the ULD configuration variables.

The resulting pipeline is: twin update; FKF/FKL residual feature; margin μ_v ; envelope $\mathcal{E}_v$; forbidden set F; QUBO; annealed ULD assignment; swipe-authorized release; hash-chain commit. Each arrow is independently attested in the literature cited above; the contribution of this reconstruction is to keep the energy equations of Sections II–IV in their original algebraic form while seating them inside that pipeline.

VI. CONCLUSION

This paper has reconstructed, without altering the algebraic form of the governing energy equations, a feasibility framework for solar-assisted electric ULD logistics. An instantaneous DC-bus power balance couples' traction, auxiliary load, regenerative recovery, and photovoltaic injection. A discrete state-of-energy update with mutually exclusive charge and discharge, together with a formula-hybrid sizing relation, protects the pack. The operational object is not raw stored energy but a solar-augmented available-energy envelope over a finite horizon, further restricted by a shared-depot charger limit. Curves attached to Sections III–V make the instantaneous balance, the SoE trajectory, the envelope-versus-work test, the charger stack, the twin residual, the FKF residue spectrum, and the QUBO penalty geometrically explicit.

Around that physical core the paper has seated four information layers that the contemporary logistics literature already treats as mature components. A digital twin rehearses assignments against the envelope before dispatch. Shift-invariant, time-shift, exponentially modulated, distributional, and two-sided

FKF analysis, together with the FKL calculus, converts twin residuals and multi-echelon lead times into a stable uncertainty margin. Hash-chain provenance, a swipe controller, and power-line-carrier anti-theft signaling make envelope decisions attributable and physically enforceable. A QUBO penalty assembled from envelope and charger violations presents those decisions to a quantum annealer already used for ULD configuration. Green-logistics and Industry 5.0 requirements [5], [24], battery-technology limits [9], solar-hybrid architectures, plug-in hybrid sizing [27], intelligent-transportation feeds [29], and digital-transformation resilience [32] are not decorative citations: each one specialises a coefficient, a bound, a feed, or an institutional constraint of the same model. Constrained resilience, as used here, is therefore a precise property: after a perturbation of irradiance, payload, lead-time spectrum, or charger occupancy, the feasible set defined by (B.4), (B.8), and (B.9) remains nonempty, and the annealer still returns an assignment outside F. Future work will close the loop quantitatively calibrating $\mu_v(t)$ on measured FKF peaks, publishing the hash-chain schema, and reporting annealing time-to-feasible-solution as a function of fleet size so that the framework can be evaluated as an operational controller rather than only as an energy-aware formulation.

REFERENCES

[1] G. Eason, B. Noble, and I. N. Sneddon, "On certain integrals of Lipschitz-Hankel type involving products of Bessel functions," Phil. Trans. Roy. Soc. London, vol. A247, pp. 529–551, April 1955.

[2] J. Clerk Maxwell, A Treatise on Electricity and Magnetism, 3rd ed., vol. 2. Oxford: Clarendon, 1892, pp. 68–73.

[3] S. Jacobs and C. P. Bean, "Fine particles, thin films and exchange anisotropy," in Magnetism, vol. III, G. T. Rado and H. Suhl, Eds. New York: Academic, 1963, pp. 271–350.

[4] Akarshan Gulhane, "Digital Twin Technology for Building Resilient and Adaptive Global Supply Chains: A Review," International Research Journal of Modernization in Engineering Technology and Science, vol. 6, no. 12, 2024, doi: 10.56726/IRJMETS64992.

[5] Akarshan Gulhane, "Artificial Intelligence Applications in Sustainable Logistics and Green Supply Chain Management: A Bibliometric Review," International Research Journal of Modernization in Engineering Technology and Science, vol. 6, no. 12, 2024, doi: 10.56726/IRJMETS65006.

[6] Akarshan Gulhane, "Artificial Intelligence and Blockchain Integration for Enhancing Supply Chain Transparency, Traceability, and Resilience," International Research Journal of Modernization in Engineering Technology and Science, vol. 6, no. 12, 2024, doi: 10.56726/IRJMETS65016.

[7] Akarshan Gulhane, "SWIPE CONTROLLER," International Journal of Research in Engineering and Applied Sciences (IJREAS), vol. 4, no. 12, pp. 1–7, 2014.

[8] Akarshan Gulhane, "Navigating the Quantum Revolution in Logistics: Opportunities and Practical Applications in Supply Chain Management," International Journal of Engineering and Techniques, vol. 12, no. 3, pp. 553–556, 2026, doi: 10.29126/ijet.2026.v12.i3.553.

[9] Akarshan Gulhane, "Recent Advances in Electric Vehicle Battery Technologies: Materials, Management Systems, and Sustainability Perspectives," International Journal of Scientific Research in Engineering and Management (IJSREM), vol. 9, no. 7, 2025, doi: 10.55041/IJSREM51198.

[10] Akarshan Gulhane, "Spectral Analysis for Multi-Scale Supply Chain Dynamics and Residue-Based Resonance Extraction in Hybrid-Vehicle Systems," Int. J. Creative Open Res. Eng. Manage., vol. 2, no. 8, 2026, doi: 10.55041/ijcope.v2i8.141.

[11] Akarshan Gulhane, "Shift-Invariant Spectral Analysis of Multi-Echelon Supply-Chain Lead Times via the FKF Transform," International Journal of Creative and Open Research in Engineering and Management, vol. 2, no. 8, 2026, doi: 10.55041/ijcope.v2i8.136.

[12] Akarshan Gulhane, "Spectral Framework Based on the FKF Transform for Supply Chain Dynamics and Resilience," International Journal of Creative and Open Research in Engineering and Management, vol. 2, no. 8, 2026, doi: 10.55041/ijcope.v2i8.140.

[13] Akarshan Gulhane, "Spectral Differential Properties of the Distributional FKF Transform with Applications to Resilient Supply-Chain Systems," International Journal of Creative and Open Research in Engineering and Management, vol. 2, no. 8, 2026, doi: 10.55041/ijcope.v2i8.139.

[14] Akarshan Gulhane, "FKL Transform Key Properties, And Applications To Supply-chain Analysis," International Journal of Engineering Sciences and Advanced Technology, vol. 25, no. 12, pp. 596–605, 2025, doi: 10.64771/ijesat.2025.v25.i12.3816.

[15] Akarshan Gulhane, "Expanded Treatment Of the Time-Shift Property Of FKF Transform With Supply-Chain Applications," International Journal of Engineering Sciences and Advanced Technology, vol. 25, no. 12, pp. 606–616, 2025, doi: 10.64771/ijesat.2025.v25.i12.3817.

[16] S. M. Harle, "Artificial Intelligence for Supply Chain Risk Prediction and Mitigation: A Systematic Review, Conceptual Framework, and Future Research Agenda," International Research Journal of Modernization in Engineering Technology and Science, vol. 8, pp. 70–80, July 2026.

[17] S. M. Harle, "Artificial Intelligence-Driven Framework for Village-Level Water Conservation and Groundwater Sustainability," International Research Journal of Modernization in Engineering Technology and Science, vol. 8, pp. 31–49, July 2026.

[18] S. M. Harle et al., "Artificial Intelligence Approaches for Strength Prediction and Optimization of Composite Concrete Mixtures: A Systematic Review and Future Research Framework," International Research Journal of Modernization in Engineering Technology and Science, vol. 8, pp. 81–97, July 2026.

[19] S. M. Harle et al., "Artificial Intelligence-Based Pavement Crack Detection: A Comprehensive Review of Machine Learning and Deep Learning Techniques," International Research Journal of Modernization in

Engineering Technology and Science, vol. 8, pp. 50–69, July 2026.

[20] S. M. Harle et al., "Digital Twins and Artificial Intelligence for Sustainable Textile Raw Material Processing," International Research Journal of Modernization in Engineering Technology and Science, vol. 8, pp. 14–30, July 2026.

[21] S. M. Harle, "Investigation of Mechanical Behavior of Steel Fiber-Reinforced Geopolymer Concrete Under Multi-Axial Stress Conditions," in Hydraulic and Civil Engineering Technology IX: Proceedings of the 9th International Technical Conference on Frontiers of HCET, Sanya, China, SAGE Publications, 25–27 September 2024, pp. 555–561.

[22] Akarshan Gulhane, "The FKF Transform: Exponential Modulation Properties and Applications to Secure Digital Supply-Chain Networks," Int. J. Eng. Sci. Adv. Technol., vol. 25, no. 12, pp. 617–623, 2025, doi: 10.64771/ijesat.2025.v25.i12.3818.

[23] Akarshan Gulhane, "Internet of Things, Artificial Intelligence, and Quantum Computing: A Convergent Framework for Smart Logistics Ecosystems," International Journal of Engineering Science and Advanced Technology (IJESAT), vol. 24, no. 12, pp. 297–317, 2024, doi: 10.64771/ijesat.2024.v24.i12.3372.

[24] Akarshan Gulhane, "Industry 5.0 and Intelligent Logistics: Transforming Supply Chain Operations through Human-Centric Automation," International Journal of Engineering Science and Advanced Technology (IJESAT), vol. 24, no. 12, pp. 287–296, 2024, doi: 10.64771/ijesat.2024.v24.i12.3371.

[25] Akarshan Gulhane, "The Future of Vehicles: Solar-Powered Battery Electric Hybrid Vehicle Architecture," Tech Briefs Create the Future Design Contest, Automotive and Transportation, entry 10457, 2020. Available: https://contest.techbriefs.com/2020/entries/automotive-transportation/10457

[26] Akarshan Gulhane, "Power line carrier communication based anti-theft system," International Journal of Research in IT and Management, vol. 4, no. 12, pp. 1–11, 2014.

[27] Akarshan Gulhane, "Battery sizing for plug-in hybrid electric vehicles — Formula hybrid," in Proc. 2017 IEEE International Conference on Power, Control, Signals and Instrumentation Engineering (ICPCSI), 2017, pp. 368–372, doi: 10.1109/ICPCSI.2017.8392317.

[28] Akarshan Gulhane, "Quantum Computing for Logistics Optimization: Annealing in Unit Load Device Configuration and Disruption," International Journal of Research Publication and Reviews, vol. 7, no. 6, pp. 4643–4648, 2026, doi: 10.55248/gengpi.07.0626.16a57.

[29] Akarshan Gulhane, "Smart Mobility and Intelligent Transportation Systems: Emerging Trends, Technologies, and Challenges," International Journal of Scientific Research in Engineering and Management (IJSREM), vol. 9, no. 11, 2025, doi: 10.55041/IJSREM53436.

[30] Akarshan Gulhane, "Quantum Computing in Transportation and Logistics: Current State, Industrial Applications, and Future Directions," International Journal of Scientific Research in Engineering and Management (IJSREM), vol. 9, no. 9, 2025, doi: 10.55041/IJSREM52469.

[31] Akarshan Gulhane, "Solar-Assisted Electric Mobility: Design Framework and Performance Assessment of Sustainable Hybrid Vehicle Architectures," International Journal of Engineering Research and Science & Technology, vol. 21, no. 3, pp. 362–368, 2025, doi: 10.56636/ijerst.2025.v21.i03.3594.

[32] Akarshan Gulhane, "Supply Chain Resilience in the Era of Digital Transformation: A Systematic Literature Review and Research Agenda," International Journal of Engineering Research and Science & Technology, vol. 21, no. 4, pp. 1058–1068, 2025, doi: 10.56636/ijerst.2025.v21.i04.3812.

[33] Akarshan Gulhane, "Distributional Extension of the FKF Transform and Its Relevance to Supply-Chain Systems," International Journal of Creative and Open Research in Engineering and Management, vol. 2, no. 8, 2026, doi: 10.55041/ijcope.v2i8.137.

[34] Akarshan Gulhane, "Sequential Convergence in the Testing Function Space of the Two-Sided FKF Transform," International Journal of Creative and Open Research in Engineering and Management, vol. 2, no. 8, 2026, doi: 10.55041/ijcope.v2i8.138.

[35] H. M. Ozaktas, Z. Zalevsky, and M. A. Kutay, The Fractional Fourier Transform. Wiley, 2001.